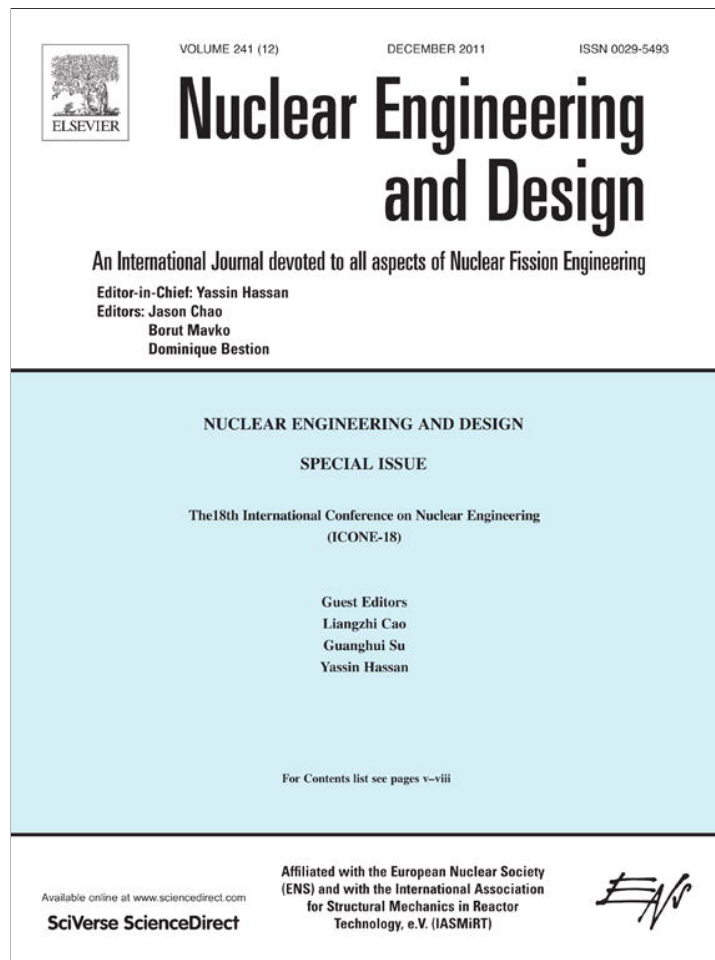


Provided for non-commercial research and education use.
Not for reproduction, distribution or commercial use.



This article appeared in a journal published by Elsevier. The attached copy is furnished to the author for internal non-commercial research and education use, including for instruction at the authors institution and sharing with colleagues.

Other uses, including reproduction and distribution, or selling or licensing copies, or posting to personal, institutional or third party websites are prohibited.

In most cases authors are permitted to post their version of the article (e.g. in Word or Tex form) to their personal website or institutional repository. Authors requiring further information regarding Elsevier's archiving and manuscript policies are encouraged to visit:

<http://www.elsevier.com/copyright>



Contents lists available at SciVerse ScienceDirect

Nuclear Engineering and Design

journal homepage: www.elsevier.com/locate/nucengdes

CFD studies on the phenomena around counter-current flow limitations of gas/liquid two-phase flow in a model of a PWR hot leg

Deendarlianto^{a,b,*}, Thomas Höhne^a, Dirk Lucas^a, Christophe Vallée^a, Gustavo Adolfo Montoya Zabala^c

^a Helmholtz-Zentrum Dresden-Rossendorf e.V., Institute of Safety Research, P.O. Box 510 119, D-01314 Dresden, Germany

^b Department of Mechanical & Industrial Engineering, Faculty of Engineering, Gadjah Mada University, Jalan Grafika No. 2, Yogyakarta 55281, Indonesia

^c Department of Chemical Engineering, Simón Bolívar University, Valle of Sartenejas, Caracas 1080, Venezuela

ARTICLE INFO

Article history:

Received 6 April 2011

Received in revised form 24 August 2011

Accepted 24 August 2011

ABSTRACT

In order to improve the understanding of counter-current two-phase flow and to validate new physical models, CFD simulations of a 1/3rd scale model of the hot leg of a German *Konvoi* pressurized water reactor (PWR) with rectangular cross section were performed. Selected counter-current flow limitation (CCFL) experiments conducted at Helmholtz-Zentrum Dresden-Rossendorf (HZDR) were calculated with ANSYS CFX using the multi-fluid Euler–Euler modelling approach. The transient calculations were carried out using a gas/liquid inhomogeneous multiphase flow model coupled with a shear stress transport (SST) turbulence model.

In the simulation, the drag law was approached by a newly developed correlation of the drag coefficient (Höhne and Vallée, 2010) in the Algebraic Interfacial Area Density (AIAD) model. The model can distinguish the bubbles, droplets and the free surface using the local liquid phase volume fraction value. A comparison with the high-speed video observations shows a good qualitative agreement. The results indicate also a quantitative agreement between calculations and experimental data for the CCFL characteristics and the water level inside the hot leg channel.

© 2011 Elsevier B.V. All rights reserved.

1. Introduction

Two-phase flow may occur in pressurized water reactors (PWR) following a leakage in the primary cooling circuit. In the event of hypothetical accident scenarios in PWR, emergency strategies have to be mapped out, in order to guarantee the reliable removal of decay heat from the reactor core, also in case of component breakdown. One essential passive heat removal mechanism is the reflux-condenser mode. This mode can appear for instance during a small break loss-of-coolant-accident (LOCA) or because of loss of residual heat removal (RHR) system during mid loop operation at plant outage after the reactor shutdown.

In the hypothetical accident scenario of a loss-of-coolant-accident (LOCA) due to the leakage at any location in the primary circuit, it is expected that the reactor will be depressurized and vaporization will take place, thereby creating steam in the PWR primary side. Should this lead to “reflux condensation”, which may be a favourable event progression, the generated steam will flow to the steam generator through the hot leg. This steam will condense

in the steam generator and the condensate will flow back through the hot leg to the reactor, resulting in counter-current steam/water flow. In some scenarios, the success of core cooling depends on the behaviour of this counter-current flow (Deendarlianto et al., submitted for publication).

In the reflux-condenser mode, a part of the condensate will flow back to the reactor core in counter-current to the steam flow. The counter-current flow of steam and condensate is only stable for a certain range of mass flow rates. If the steam mass flow rate increases too much, the condensate is clogged in the hot leg. The condensate is carried over by the steam and partially entrained in the opposite direction to the steam generator. This phenomenon is known as the counter-current flow limitation (CCFL) or flooding, and could affect the cooling of the reactor core. Detailed examples of such LOCA scenarios leading to the reflux condenser mode can be found in Jeong (2002).

A lot of experiments were carried in the past in order to understand the phenomena around CCFL in a model of hot leg PWR. Several experimental correlations were developed to predict the CCFL on them, but they are only valid in specific experimental ranges. Therefore, high resolution experimental data at reactor typical boundary conditions is needed. In order to improve the transient analysis of counter-current two-phase flows, experimental studies were conducted at Helmholtz-Zentrum Dresden-Rossendorf (HZDR). A 1/3rd scale model of the hot leg of

* Corresponding author at: Helmholtz-Zentrum Dresden-Rossendorf e.V., Institute of Safety Research, P.O. Box 510 119, D-01314 Dresden, Germany.
Tel.: +49 351 260 3291; fax: +49 351 260 13291.

E-mail addresses: deendarlianto@ugm.ac.id, d.deen@hzdr.de (Deendarlianto).

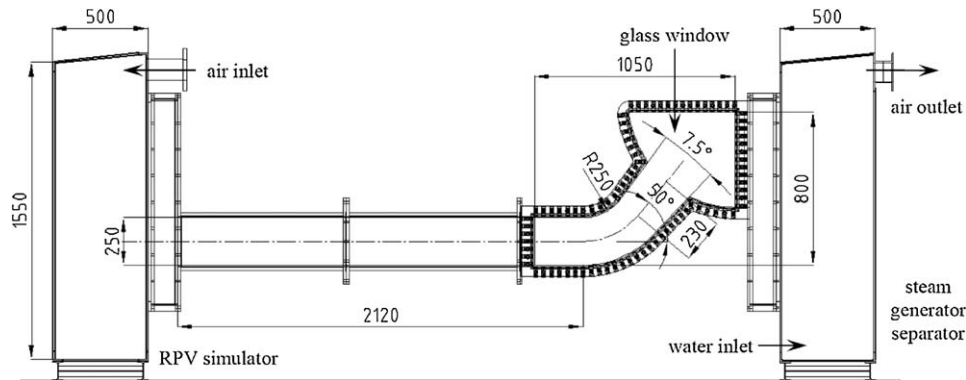


Fig. 1. Schematic drawing of the hot leg model test section (dimension: in mm) (Deendarlianto et al., 2008).

a German Konvoi PWR with rectangular cross section was used (Deendarlianto et al., 2008; Vallée et al., 2009a).

The nuclear thermal-hydraulic community is facing today interesting challenges. These include the development and validation of new computational tools that will be used for improved and more detailed analysis as well as new generations of reactors. Current trends are toward multi-dimensional, -scale, -physics approaches for such analyses (Yadigaroglu, 2005). For this purpose, the computational fluid dynamics (CFD) tool is considered to be able to simulate most of two-phase flow configurations encountered in nuclear reactor power plants.

The most widely used analysis to model the CCFL in a PWR hot leg is based on the one dimensional two-fluid models as reported by Ardron and Baneerjee (1986), Lopez de Bertodano (1994) and Wongwises (1996). In this approach, the switching point, where the flow condition changes from sub to critical condition in stratified flow is approached by the experimental correlation in a specified flow direction. Wang and Mayinger (1995) did two-dimensional analyses of counter-current model of UPTF Test TRAM A2 & Test 11 using a two-fluid model. They implemented the interfacial friction factor proposed by Lee and Bankoff (1983) and Ohnuki (1986) into the code FLOW3D. They reported that satisfactory results were obtained, whereas, under the reflux condensation conditions, numerical computation reveals that different flow structures appeared in the region away from the flooding curve and in the region near the flooding curve.

Murase and his co-workers in Tsuruga-Japan are in disagreement with the study of Wang and Mayinger. They claimed that the effects of wall friction can not be correctly evaluated by using two-dimensional analysis. The given boundary conditions at the inlet and outlet of the hot leg in the above work might affect the calculated flow patterns in the hot leg. For this reason they conducted 3-D CFD calculations. Their CFD works can be found in Murase et al. (2009), Minami et al. (2009, 2010b), Kinoshita et al. (2009), and Utanohara et al. (2009).

Murase et al. (2009), Minami et al. (2009, 2010b) and Utanohara et al. (2009) conducted 3-D CFD simulations on counter-current flow in a PWR hot-leg air-water two-phase flow in a 1/15th scale model. This calculation model reproduced the size of experimental test facility at Kobe University as reported by Minami et al. (2010a). Their works included the effects of interfacial friction correlation (Utanohara et al., 2009), flow patterns and CCFL (Murase et al., 2009; Minami et al., 2009, 2010b). They used the volume of fluid (VOF) and Euler–Euler two-fluid models on the commercial CFD code FLUENT6.3.26. The required interfacial friction correlations in the Euler–Euler two-fluid model were selected from a combination of available 1-D experimental correlations for the cases of annular and slug flow that gave the best agreement with the experimental data. They concluded that it is better to use the two-fluid model

with suitable interface friction correlation than VOF model. The predicted flow patterns, hysteresis behaviours, and CCFL characteristics agree well with their experimental data. Meanwhile those correlations were obtained on the basis of one dimensional analysis, which might affect the calculation results. The use of the 1-D experimental correlation to the 3-D problem might be not accurate when we look into the local physics of the phenomenon.

The development of a general model closer to physics and including less empiricism is a long-term objective of the HZDR research programs. Here local geometry independent models for mass, momentum, heat transfer, and scalar transport are developed and validated. Such models are an essential precondition for the application of CFD codes to the modelling of flow related phenomena in nuclear facilities. One of the developed scientific methods to solve the above problems was the new concept of drag coefficient in the algebraic interfacial area density model (AIAD) (Höhne, 2009).

The aim of this paper is to simulate the phenomena around the CCFL in a PWR hot leg with newly developed of new concept of drag coefficient in the AIAD model to the Euler–Euler problem. It allows the detection of the morphological form of the two phase flow and the corresponding switching via a blending function of each correlation from one object pair to another. The new drag correlation in this model considers the 3D effects of the simulated phenomenon.

2. Experimental apparatus and procedures

The details of the experimental apparatus and procedure used in the present study were described in the previous papers (Deendarlianto et al., 2008; Vallée et al., 2009a) and only the main features are presented here. Fig. 1 shows a schematic drawing of the test section. The tested fluids were air–water and saturated steam–water. Two vessels simulate the reactor pressure vessel (RPV) simulator and steam generator (SG) separator are connected by a test section that simulates the 1/3rd scale model of the hot leg PWR of a German Konvoi Pressurized Water Reactor. Both vessels are identical vessels with $0.8 \text{ m} \times 0.5 \text{ m} \times 1.55 \text{ m}$ ($D \times W \times H$) cubic shape. The water level in both vessels was determined by the measurement of the differential pressure between the top and the bottom of the vessels with differential pressure transducers. A vortex meter was used to measure the injected water mass flow rate. The injected air mass flow rate was measured and controlled using a thermal mass flow meter, the steam flow rate over the pressure drop through an ISA nozzle.

The test section is composed of a horizontal rectangular channel, a bend that connects it to an upward inclined and expended channel, and a quarter of a circle representing the steam generator inlet chamber. The horizontal part of test section is 2.12 m long and has a rectangular cross-section of $0.05 \text{ m} \times 0.25 \text{ m}$. The riser is

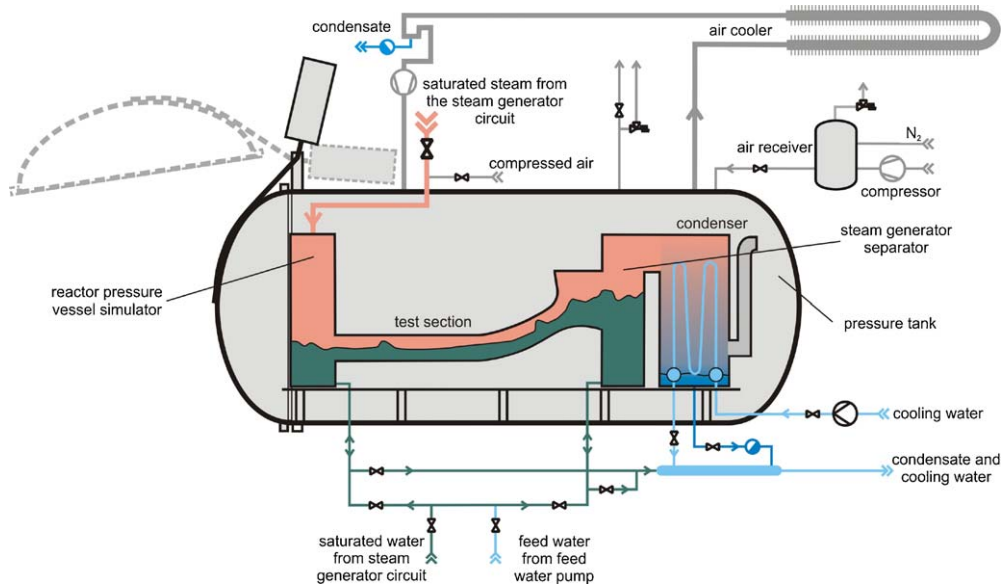


Fig. 2. Schematic diagram of the experimental apparatus (Deendarlianto et al., 2008).

0.23 m long, has an inclination of 50° to the horizontal plane and an expansion angle of 7.5° . The inner and outer bend radii of curvature were 0.25 and 0.5 m, respectively. Unfortunately, due to the overall dimensions of the hot leg model, it was not possible to visualize the complete test section. Therefore, a region of observation had to be chosen. Previous investigations (e.g. Ohnuki et al., 1988) indicate that the most agitated flow region is located near the bend and that a recirculation zone forms there. Consequently, it was chosen to observe the bended region of the hot leg and the steam generator inlet chamber as shown in Fig. 1. The flow behaviour was recorded by a high-speed video camera at frequencies of 60–100 Hz and a shutter speed of 1/500 to 1/1000 s.

This experimental apparatus is put in a pressure tank, where it was operated in pressure equilibrium with the inner atmosphere of the tank as shown in Fig. 2. The photo of the hot leg model is shown in Fig. 3. Air and nitrogen were injected to increase the pressure in the tank to a maximum operation pressure of 5.0 MPa of the air–water and the steam–water experiments respectively. The detailed principle of the pressure equilibrium technique was described by Prasser et al. (2006) and Vallée et al. (2009b).

In the experiment, a constant water flow rate was injected at the bottom of the SG simulator from where it can flow through the test section to the RPV simulator. The gas was injected into the RPV simulator from the top and flowed through the test section in counter-current to the water flow to the SG separator. The increase of the water level in the RPV simulator was used to determine the water flow rate streaming over the test section (discharge flow). The onset of flooding was defined as the limiting point of stability

of the counter-current flow, indicated by the maximum air mass flow rate at which the down-flowing water mass flow rate is equal to the inlet water mass flow rate.

3. Computational modelling

In the present simulation, the flow was treated as transient. The problem is three dimensional (3-D), consequently, it has to be solved by applying computational fluid dynamics (CFD) methods. Such multiphase codes resolve the conservation equations for



Fig. 3. Hot leg model at the TOPFLOW test facility.

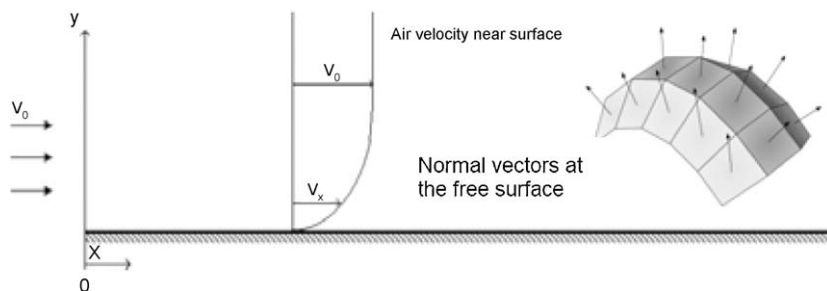


Fig. 4. Air velocity near the free surface (Höhne and Vallée, 2010).

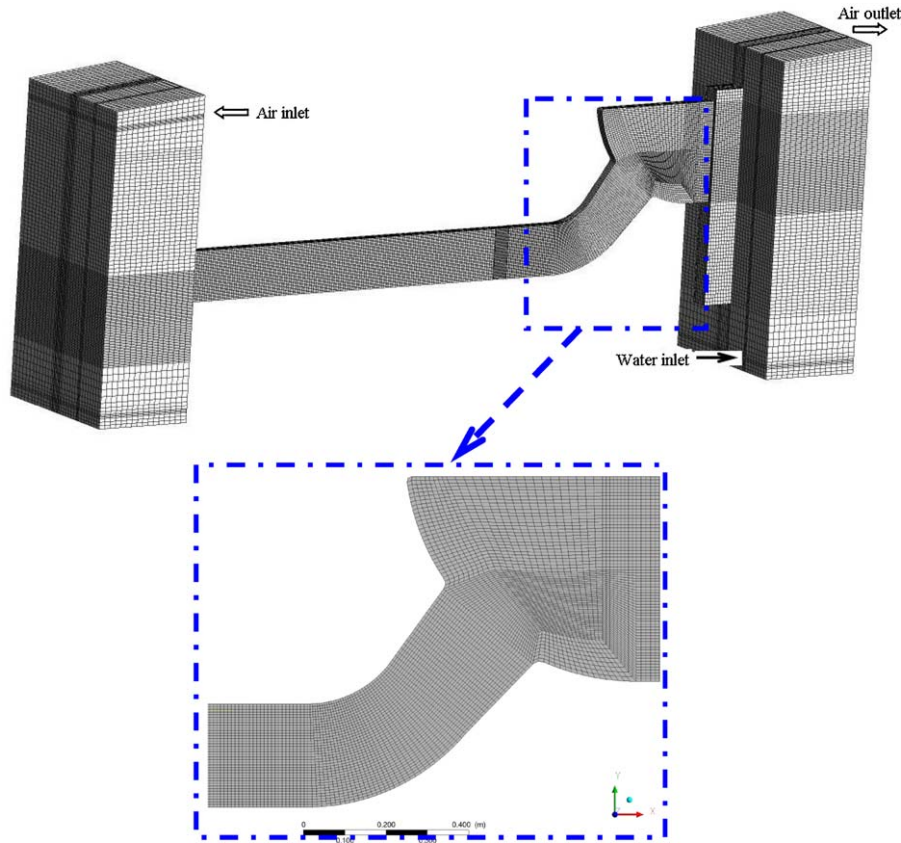


Fig. 5. Calculation model.

mass, momentum and energy and they are distinguished by the different approaches and strategies used in describing the physical closure models. For the solution of the described task, an Euler–Euler approach was used.

The Euler–Euler approach assumes that at least two fluids are continuously penetrating each other. The volume fraction of the fluids in each cell sums to unity. For each fluid, the full set of conservation equations is solved. The mechanisms of interaction between the fluids are the momentum transfer modelled by the flow resistance, the mass transfer modelled by phase change and the energy transfer modelled by heat conduction. Both phases are assumed to be adiabatic and incompressible; therefore, the two latter interactions in the present problem are not relevant in the present problem.

In the present simulation, we solve the conservation and momentum equations of the two-fluid model, which have the following form

$$\frac{\partial(\alpha_k \rho_k)}{\partial t} + \nabla(\alpha_k \rho_k U_k) = 0 \quad (1)$$

$$\frac{\partial(\alpha_k \rho_k)}{\partial t} + \nabla(\alpha_k \rho_k U_k U_k) = -\alpha_k \nabla p_k + \alpha_k \rho_k g + \nabla \alpha_k (\tau^v + \tau_k^t) + \tau_{D,k} \quad (2)$$

where the subscript k denotes phase gas or liquid, ρ is the density, u is the velocity vector, t is the time, p is the pressure, g is the gravitational acceleration, α is the volume fraction, τ is the shear stress (τ^v is the average viscous shear stress and τ^t is the turbulent shear stress) and τ_D is the interfacial shear stress.

The drag force is derived from the interfacial shear stress ($F_D = \tau_D \cdot A$), is most conveniently expressed in terms of the drag coefficient C_D

$$F_D = C_D A \rho_{LG} |U_L - U_G|^2 \quad (3)$$

where ρ_{LG} is the average density, $|U_L - U_G|$ is the relative velocity and A is the projected area of the body in flow direction (interfacial area density). In the present work, the capabilities of the C_D in AIAD model and will be examined.

3.1. Free surface and AIAD model

In the previous experimental paper (Deendarlianto et al., 2008) it was reported that there are three morphologies at CCFL condition. Those are bubble flow, stratified flow with a free surface and entrainment liquid droplet. Höhne and Vallée (2010) noted that the CFD simulation of the free surface can be performed by using the multi-fluid Euler–Euler modelling approach available in ANSYS CFX. However it requires a careful treatment of several aspects of

Table 1
Calculation runs.

Exp. run	Drag coefficient	\dot{m}_L [kg/s]	Range of \dot{m}_G [kg/s]	Pressure [MPa]
30-09 (air/water)	$C_D = 0.44$	0.3	0.183–0.274	0.15
	AIAD	0.3	0.183–0.274	0.15
11-01 (steam/water)	AIAD	0.3	0.490–0.669	1.50

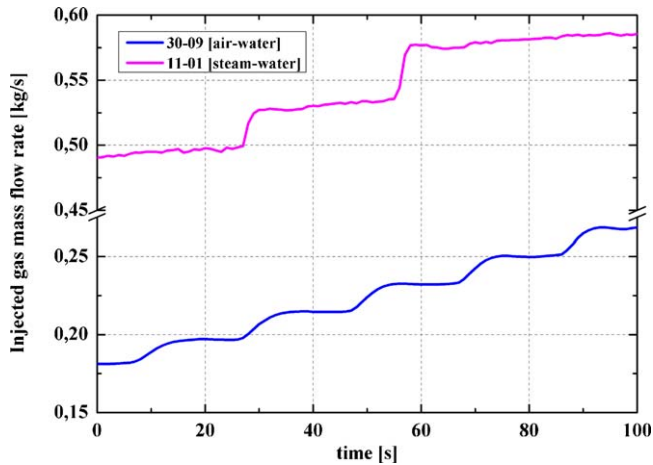


Fig. 6. Injected gas mass flow rate as a function of time according to experimental injected gas flow rates profiles.

the model. Those are interfacial area density, turbulence model near free surface and inter-phase momentum models. The separate models are also necessary for dispersed particles and separated continuous phases (interfacial drag, etc.).

The suitable methodology within the Euler–Euler approach is to use the momentum exchange coefficient depends on the local morphology. For that reason, Yegorov (2004) proposed an Algebraic Interfacial Area Density (AIAD) model to solve the above problem. The basic conceptions of the proposed model are:

- The interfacial area density allows the detection of the morphological form and the corresponding switching for each correlation from one object pair to another.
- It provides a law for interfacial area density and the drag coefficient for full range of $0 \leq \alpha_L \leq 1$.

- The interfacial area density in the intermediate range is set to the interfacial area density for the free surface.

The interfacial area density A also depends on the morphology of the phases. For bubbles, the interfacial area density is defined as follows

$$A_B = \frac{6\alpha_G}{d_B} \quad (4)$$

Here d_B is the bubble diameter and α_G is the gas void fraction.

For a free surface an important requirement for the model is the normalizing condition: the volume integral of the area density must be equal to the real surface area. It means that integration of the area density along a normal to the surface must yield unity:

$$\int_{-\infty}^{+\infty} A \, dn = 1 \quad (5)$$

For a free surface, the interfacial area density is defined as absolute value of the gradients of the liquid fraction in x , y and z directions, and is written as

$$A_{FS} = |\nabla\alpha_L| = \sqrt{\left(\frac{\partial\alpha_L}{\partial x}\right)^2 + \left(\frac{\partial\alpha_L}{\partial y}\right)^2 + \left(\frac{\partial\alpha_L}{\partial z}\right)^2} \quad (6)$$

Next, the average density ρ_{LG} is defined as

$$\rho_{LG} = \rho_G\alpha_G + \rho_L(1 - \alpha_G) \quad (7)$$

where ρ_L and ρ_G are the liquid and gas densities, respectively. In the bubble regime, where the α_G is low, the average density according to Eq. (7) is close to liquid phase density ρ_L . According to the flow regime (bubbly flow, droplet flow or stratified flow with a free surface), the corresponding drag coefficients and area densities have to be applied. This problem can be solved by introducing a blending function f . Introducing void fraction limits, the blending function

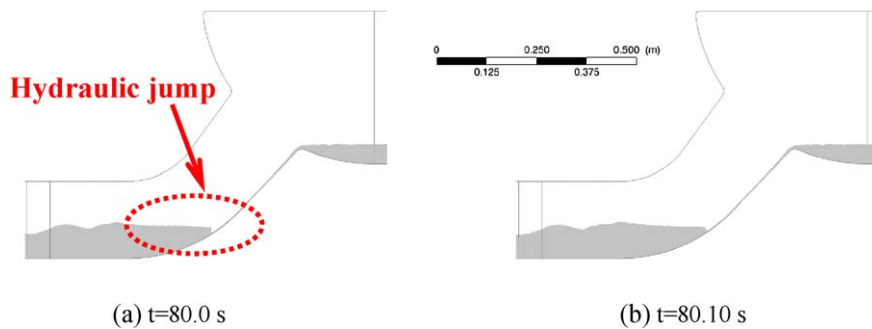
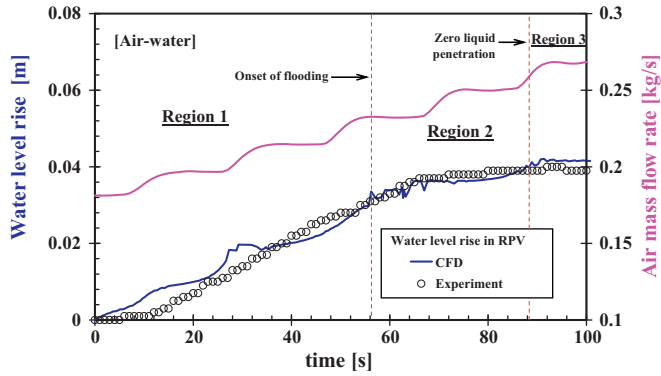


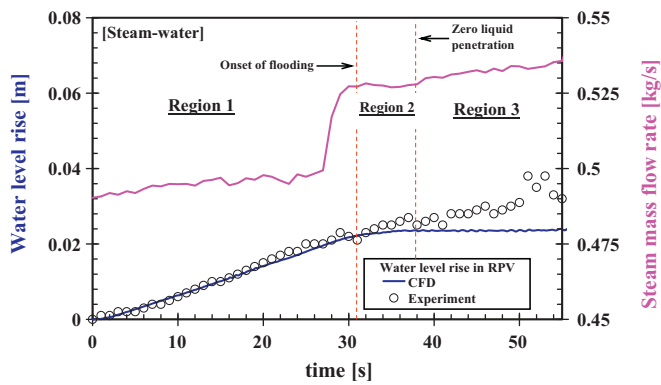
Fig. 7. Calculated liquid level in hot leg channel using $C_D = 0.44$ (air–water, $\dot{m}_L = 0.30$ kg/s and $\dot{m}_G = 0.25$ kg/s).



Fig. 8. Interfacial behaviour of air–water in hot leg channel during flooding (air–water, $\dot{m}_L = 0.30$ kg/s and $\dot{m}_G = 0.25$ kg/s).



(a) Air-water (HZDR experimental run of 30-09)



(b) Steam-water (HZDR experimental run of 11-01)

Fig. 9. Evolution of the water level in the RPV simulator in function of the gas flow rate ($\dot{m}_G = 0.30$ kg/s).

and length scales for bubbly and droplet regimes are respectively defined as

$$f_B = \frac{1}{1 + e^{A_B(\alpha_G - \alpha_{B,limit})}} \quad (8)$$

$$f_D = \frac{1}{1 + e^{A_D(\alpha_G - \alpha_{D,limit})}} \quad (9)$$

Next, the blending function for the free surface is defined as

$$f_{FS} = 1 - f_B - f_D \quad (10)$$

Then, the area density and the drag coefficient are respectively well defined in the domain by

$$A = f_{FS}A_{FS} + f_B A_B + f_D A_D \quad (11)$$

$$C_D = f_{FS}C_{D,FS} + f_B C_{D,B} + f_D C_{D,D} \quad (12)$$

After a validation study for this work the void fraction limits of $\alpha_{B,limit} = 0.3$ respectively $\alpha_{D,limit} = 0.7$ and blending coefficients of $\alpha_B = \alpha_D = 70$ were used.

In simulation of free surface flows, Eq. (3) does not represent a realistic physical model. It is reasonable to expect that the velocities of both fluids in the vicinity of the interface are rather similar. To achieve this result, it is assumed that the shear stress near the surface behaves like a wall shear stress on both sides of the interface in order to reduce the velocity differences of both phases.

Höhne and Vallée (2010) derived a drag coefficient in the AIAD model for the free surface application. In their proposal, a shear stress like a wall shear stress is assumed near the surface from both sides to reduce the velocity differences of both phases as shown in Fig. 4. Here, a viscous fluid moving along a “solid” like boundary will incur a shear stress, the no-slip condition, the morphology region “free surface” is the boundary layer, the shear stress is imparted onto the boundary as a result of this loss of velocity.

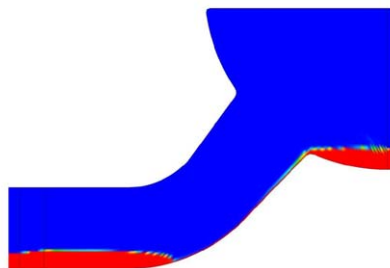
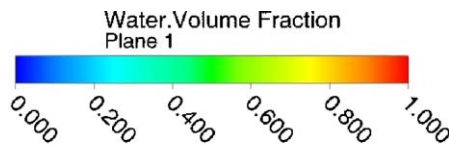
$$\tau_{W,i} = \mu_i \frac{\partial u_i}{\partial y} \Big|_{y=0} \quad (13)$$

Finally, the drag coefficient of the free surface can be obtained from the substitution of the Eqs. (3), (6) and (13) and is locally dependent on the fraction of phases, liquid density, and the slip velocity between the phases:

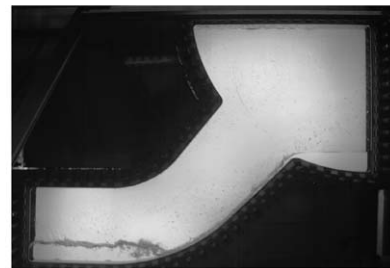
$$C_D = \frac{2(\alpha_L \tau_L + \alpha_G \tau_G)}{\rho_L (U_L - U_G)^2} \quad (14)$$

where wall shear stresses of the gas and liquid τ_L and τ_G onto the free surface are a function of the viscosity of both phases, the area of free surface and the gradient of void fraction in x, y, z axes.

In the simulation, the drag coefficient of the bubble, a constant value of $C_{D,B} = 0.44$ is taken, based on the drag of rigid spheres at the medium to high Reynolds number regime. For the drag coefficient of the droplet, the $C_{D,D} = 0.44$ is also taken. On the other hand, the drag coefficient of the free surface, $C_{D,FS}$, refers to Eq. (14).



(a) Calculated water volume fraction



(b) Visual observation obtained from experiment

Fig. 10. Flow structure of the counter-current gas/liquid two-phase flow near the elbow before flooding (air-water (30-09), $\dot{m}_G = 0.181$ kg/s, and $t = 5$ s).

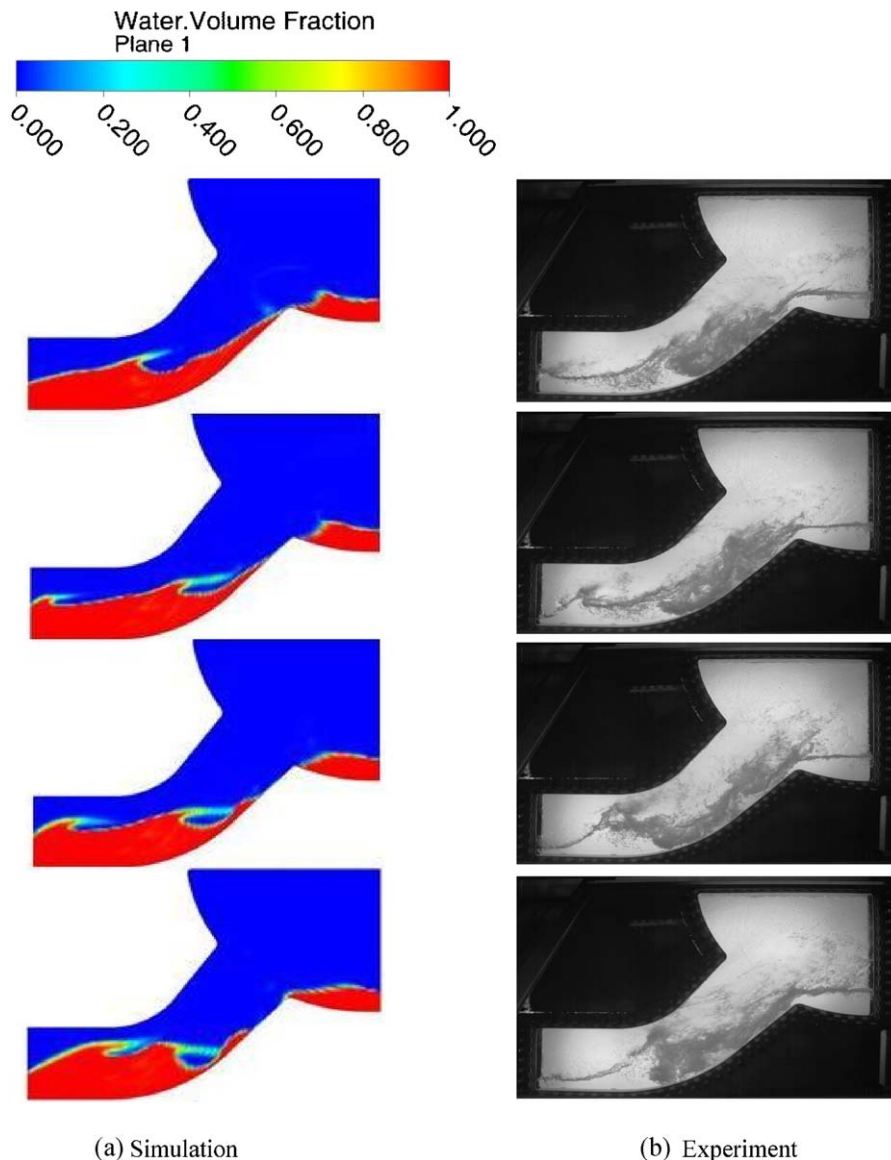


Fig. 11. Flow structure of the counter-current gas/liquid two-phase flow near the elbow around flooding ($\dot{m}_G = 0.268$ kg/s) of air–water test (HZDR experimental running of 30-09); (a) calculated water volume fraction and (b) visual observation obtained from experiment.

3.2. Computational setup and boundary conditions

Numerical errors in CFD simulation are the result of a combination of many aspects, which includes the mesh resolution, discretisation method, time step size and convergence errors. Validation of the computational models used must be made using specific or known conditions based on gathered experimental data. However, the separation of different numerical effects is difficult; for example, numerical diffusion in the flow direction can smudge or smooth the estimated values downstream of the perturbation. The effect is similar to the selection of too large a turbulent viscosity for some turbulence models. In CFD analysis, demonstration of grid independence is also a basic requirement as indicated in the ERCOFTAC Best Practice Guidelines 2001 (Menter, 2002). However, due to insufficient computer resources, in real technical problems mostly it cannot be achieved (Farkas and Tóth, 2010).

In the present work, the phenomenon of gas/liquid counter-current two-phase flow in model of a PWR hot leg was approached by using the Euler–Euler inhomogeneous model available in the commercial CFD code of ANSYS CFX 12.0. In our simulations, very

carefully developed structured mesh for most of the flow field was adequate, at which the local refinement on them was carried out. As a result, the flow domain was modelled with a structured mesh consisting of 248,610 hexahedral elements and 281,076 nodes as shown in Fig. 5.

The following parameters were used in the simulations. Both phases have treated as isothermal and incompressible. Buoyancy effects between the two-phase were taken into account by the direction of gravity term. The turbulence properties at the inlet of air and water were set using the “turbulence intensity of 5% in both phases”. The air outlet was modelled with an opening boundary condition. The inner surface of the channel walls has been defined as hydraulically smooth with a non-slip boundary condition applied to both gas and liquid phases. A time step 10^{-4} s and a maximum of 15 coefficient loop were taken to model the flow. A convergence in terms of the RMS values of the residuals to be less than 10^{-4} could be assured most of the time.

The SST buoyancy turbulence model and upwind advection scheme were used in the simulation. The SST model works by solving a turbulence/frequency-based model ($k-\omega$) at the wall

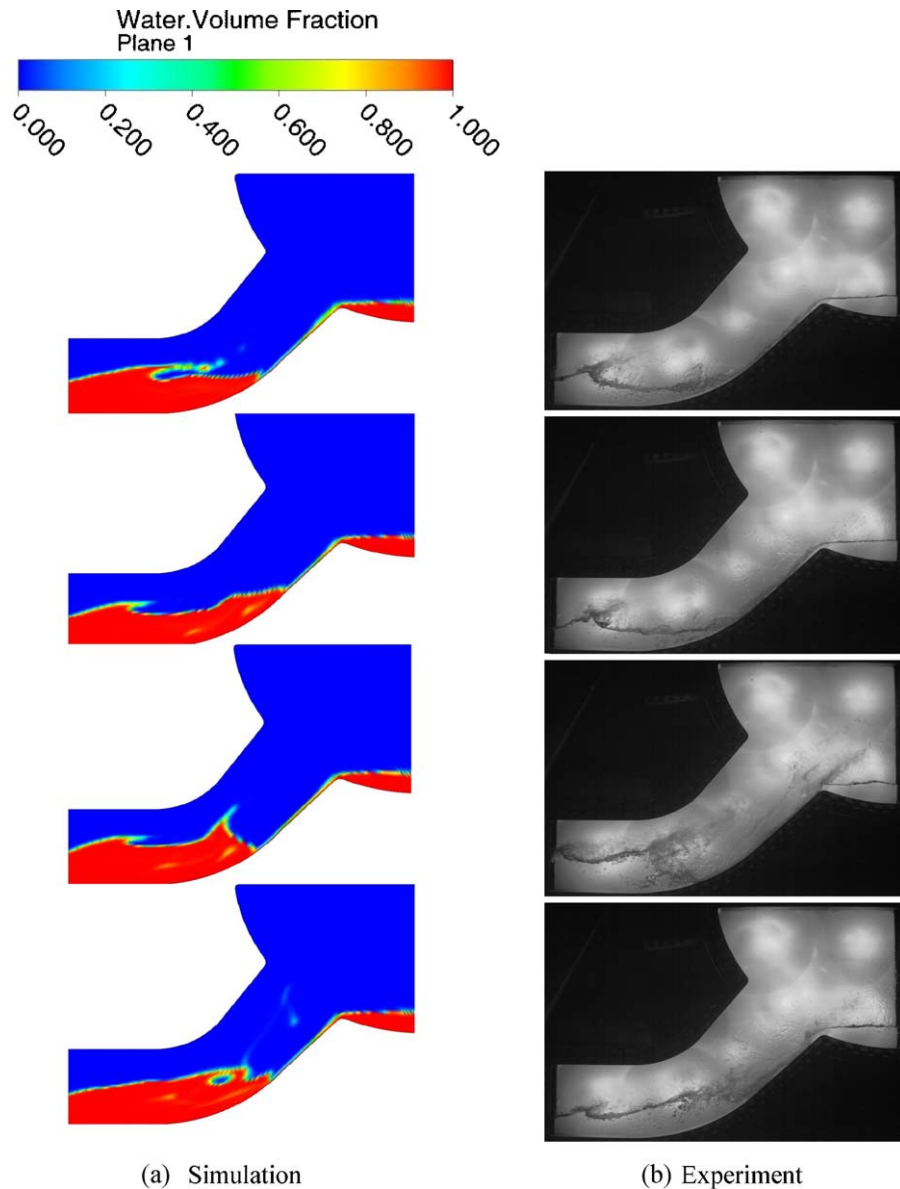


Fig. 12. Flow structure of the counter-current gas/liquid two-phase flow near the elbow around flooding ($\dot{m}_G = 0.530$ kg/s) of steam–water (HZDR experimental run of 11-01); (a) calculated water volume fraction and (b) visual observation obtained from experiment.

and standard $k-\varepsilon$ in the bulk flow. A blending function ensures a smooth transition between those two models (Menter, 1993). In the calculations, newly developed C_D in AIAD model (Eq. (14)) was implemented into ANSYS CFX12.0 via the command language CEL (CFX expression language).

Three (3) calculations of two HZDR experimental runs (30-09 and 11-01), and they are summarized in Table 1 have been performed. In the calculation, the injected gas flow rates were varied in time according to the measured gas flow rates as shown in Fig. 6. The calculations were performed in parallel of 4 processors of a Linux cluster (operating system: Linux Scientific 64 bit, 32 AMD Opteron Computer Nodes, node configuration: $2 \times$ AMD Opteron 285 (2.6 GHz, dual-core), 16 GB memory). Typical computation time for each case was about 4 months.

4. Results and discussions

A first transient simulation was carried out by using a constant of $C_D = 0.44$ for the experimental running of 30-09. This value is

applicable to the drag coefficient of a spherical particle in a liquid under turbulent regime. It was proposed by Wallis (1969) and is also a default value from ANSYS CFX. The results are shown in Fig. 7. In the figure, the calculated flow structures of the counter-current air–water two-phase flow near the elbow at high air mass flow rate ($\dot{m}_G = 0.25$ kg/s) i.e. during flooding are shown. From the transient flow simulation the predicted flow was characterized by the thin liquid film in the bend region. A hydraulic jump as the transition from supercritical to subcritical flow is observed near the bended region, which is in contradiction to the experimental observation shown in Fig. 8. In fact, the formation of liquid slugs and the entrainment of liquid droplets during flooding as observed in experiment could not be reproduced here. This result indicates that interfacial friction seems to be important at the wave crest during flooding, whereas $C_D = 0.44$ is not big enough to promote a liquid slug and break it in the hot leg channel.

For the above reason the newly developed drag coefficient in AIAD model as described in Section 3.1 was used to simulate the CCFL in a model of PWR hot leg in the following. In contrast to

the first simulation with constant C_D , the onset of CCFL can be simulated by using this model. Fig. 9 shows the calculated and experimental results of the average water level rise in the RPV simulator in function of time. In the figures, those are plotted against the corresponding experimental data of the injected gas mass flow rate. In the figure, (a) and (b) correspond to the cases of air–water and steam–water, respectively. The calculated water level rise and injected gas mass flow rate are shown by the blue and pink curves, respectively. The points correspond to measured values of the water level. From the figures, the phenomena can be explained as follows.

1. In both cases, the water level rise is similar and can be divided into three regions. In the first region, the water level increases with a constant slope independently of the injected gas mass flow rate. In the second region, the slope of the curve of water level in the RPV simulator begins to decrease. It means that a part of the water injected in the SG separator does not flow to the side of the RPV simulator anymore. This point is known as the onset of flooding (CCFL). With further increase of the gas mass flow rate, the calculated water level rise shows a plateau (region 3). This means that none of the injected water in the SG separator flows to the RPV simulator side.
2. The characteristics of the water level rise described above seem to confirm the experimental observations of Deendarlianto et al. (2008). They defined the region 1, region 2, and region 3 as the stable counter-current flow, partial delivery region and zero liquid penetration respectively. Next, it is also noticed that the calculated results are generally in agreement with the experimental data as shown in Fig. 9(a) and (b). However a minor difference of the water level between the experiment and the calculation of the steam–water case in the regions of the partial delivery and zero liquid penetration was found. In the experiment, the water level rise in the region 3 tends to increase with the time, meanwhile it is almost constant in the calculation. The difference is believed to be due to the turbulence behaviour at the interface of steam and water, such as turbulence damping effect, was not accounted in the calculation. Therefore it should be considered in the future.

Fig. 10 illustrates the flow structure of the counter-current gas/liquid two-phase flow near the elbow at low gas mass flow rate ($\dot{m}_G = 0.181 \text{ kg/s}$) i.e. before the onset of flooding for the air–water case. Here new drag coefficient in AIAD model was also applied. In the figure, (a) and (b) correspond to the calculated water volume fraction and the visual observation obtained from the experiment respectively. From Fig. 10(a), a thin liquid film was found in the bend region, and a hydraulic jump is clearly visible near the bended region, which agrees well with the experimental observation shown in Fig. 10(b).

Figs. 11 and 12 illustrate the flow structure of the counter-current gas/liquid two-phase flow near the elbow at high gas mass flow rate i.e. flooding condition for the air–water and the steam–water cases respectively. In the figure, (a) and (b) correspond respectively to the time variation of the calculated water volume fraction ($\Delta t = 0.1 \text{ s}$) and the visual observation obtained from the experiment. From the figures, it is clearly shown that a bigger wave is generated by the merging of small waves due to the interfacial drag. The entrainment of liquid droplet observed in the experiment can also be reproduced in the simulation. Here a high migration of the crests of the waves toward the steam generator in which the down-flowing liquid film is disturbed plays an important role on the backwards liquid transport during flooding.

A comparison of the flooding curves between the CFD calculation and experiment is shown in Fig. 13. For a meaningful comparison, the non-dimensional superficial velocity J_k^* , named as

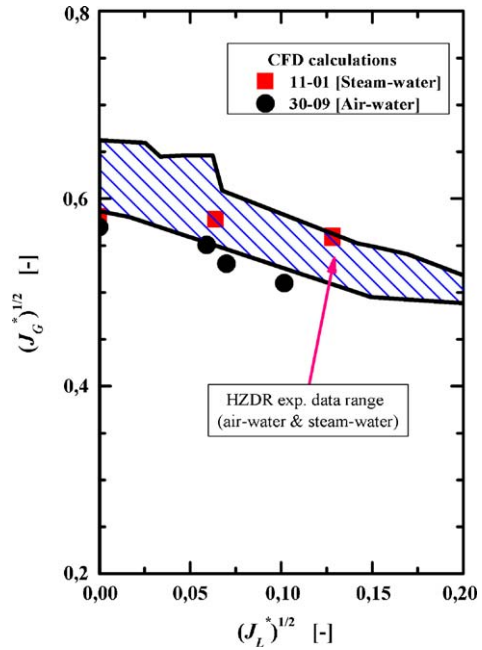


Fig. 13. CCFL characteristics.

Wallis parameter is used. Here the Wallis parameter in Fig. 13 is defined as

$$J_k^* = J_k \sqrt{\frac{1}{gH} \cdot \frac{\rho_k}{\rho_L - \rho_G}} \quad (15)$$

where the subscript k indicates gas and liquid phases, J the superficial velocity, and H the height of the channel (cf. Vallée et al., 2011). Close inspection of Fig. 13 reveals that the calculated CCFL pass through the range of HZDR experimental data, indicating a good agreement between the calculation and experimental data. A comparison between both simulation results indicates that the gas velocities at zero liquid penetration ($(J_L^*)^{1/2} = 0.0$) of both cases is almost the same. This means that there is a minor effect of the fluid viscosities on the zero liquid penetration point, whereas it is not accounted in the Wallis parameter. The same behaviour was also found by Nariai et al. (2010) experimentally. This behaviour can be explained by the fact that at this point the net-flow in the flow path is equal to zero. Therefore, liquid viscosity which mainly influences the wall and interfacial frictions does not play an important role here. Next it noticed also that the difference on the flooding curves between both cases increases with $(J_L^*)^{1/2}$. It indicates that the liquid viscosity has an increasing effect with the liquid mass flow.

In order to make a quantitative comparison of the water level inside the hot leg channel between the experiment and calculation, an interface capture method was developed (see Montoya et al., 2011). To capture the gas–liquid interface in the camera frames, an image processing algorithm was developed. This technique allows the representation of the interface by a water level as a function of locus in the channel x and the time t . Nevertheless, for a comparison between the CFD calculation and experimental result, a surface similar to the interface in the camera pictures has been defined. Therefore an *isosurface* with a void fraction of 50% was chosen and the coordinates of its intersection with the vertical mid-plane was exported from ANSYS CFX. With this simplification, the three-dimensional shape of the *isosurface* was not taken into the account.

The time-averaged water level profile for both of experiments and CFD calculations is shown in Fig. 14. In the figure, (a) and (b)

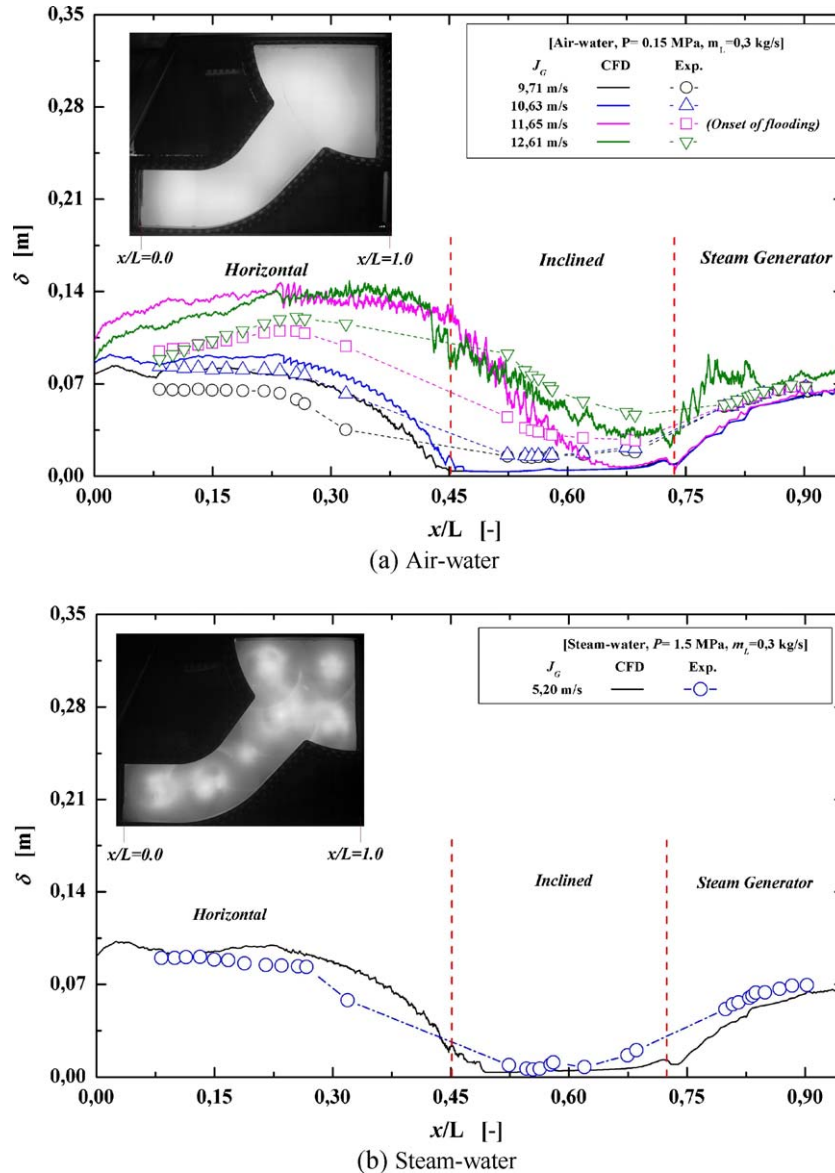


Fig. 14. The comparison on the water level inside the hot leg channel between the calculations and experiments.

correspond to the cases of air–water and steam–water, respectively. The water level data are presented as a function of location and of the superficial gas velocity. Qualitatively, Fig. 14 shows that the trend obtained for the simulation is similar to the measurement. In the experiment with air–water (Fig. 14(a)), before the onset of flooding the average water level profile in the horizontal part increases at a distance far from the inclined part. However, a detailed comparison shows a minor deviation between simulations and measurements. Possible reasons for the discrepancy are the three dimensional effects found in the water level measurement or the using inlet boundary conditions in the simulation. Therefore future works on those problems should be considered.

5. Summary

The new concept of the drag coefficient in the AIAD model was implemented to describe the whole phenomena of CCFL in a model of a PWR hot leg by applying CFD methods. The presented results showed a clear progress in the simulation of the relevant phenomena, in which only AIAD model allows the correct simulation of CCFL physically. The developed approach will also enable the

answering of many practical questions relating to the CCFL phenomenon. Moreover, further improvement of the model should be carried out. Here the usage of the morphology detection algorithm should also be possible also in vertical flow regimes. Therefore, it is necessary to include the modelling of non-drag forces (lift force, wall lubrication force, virtual mass force, etc.) in the AIAD model as well as the available for polydispersed flows. Next the turbulence damping procedures should include the existence of small surface instabilities in the macroscopic model. In addition the numerical approach of the AIAD model should be improved to further reduce the calculation time.

Acknowledgements

This work is carried out within the frame work of a current research project funded by the German Federal Ministry of Economics and Technology, project number 150 1329. The authors would like to thank also the TOPFLOW team for their work on the test facility and the preparation of the experiments.

Dr. Deendarlianto is an Alexander von Humboldt Fellow in the Institute of Safety Research, Helmholtz-Zentrum Dresden-

Rossendorf e.V., Dresden, Germany. The present research is also supported by the Alexander von Humboldt Foundation in Germany.

References

- Ardron, K.H., Baneerjee, S., 1986. Flooding in an elbow between a vertical and a horizontal or near horizontal pipe; part II: theory. *International Journal of Multiphase Flow* 12 (4), 543–558.
- Deendarlianto, Vallée, C., Lucas, D., Beyer, M., Pietruske, H., Carl, H., 2008. Experimental study on the air/water counter-current flow limitation in a model of the hot leg of a pressurized water reactor. *Nuclear Engineering and Design* 238 (12), 3389–3402.
- Deendarlianto, Höhne, T., Lucas, D., Vierow, K. Gas-liquid countercurrent two-phase flow in a PWR hot leg: a comprehensive research review. *Nuclear Engineering and Design*, submitted for publication.
- Farkas, T., Tóth, I., 2010. Fluent analysis of a ROSA cold leg stratification test. *Nuclear Engineering and Design* 240 (9), 2169–2175.
- Höhne, T., 2009. Experiments and numerical simulations of horizontal two-phase flow regimes. In: *Proceeding of the Seventh International Conference on CFD in the Minerals and Process Industries*, Melbourne, Australia.
- Höhne, T., Vallée, C., 2010. Experimental and numerical simulations of horizontal two-phase flow regimes using an interfacial area density model. *The Journal of Computational Multiphase Flow* 2 (3), 131–143.
- Jeong, H.Y., 2002. Prediction of counter-current flow limitation at hot leg pipe during a small break LOCA. *Annals of Nuclear Energy* 29 (5), 571–583.
- Kinoshita, I., Utanohara, Y., Murase, M., Minami, N., Tomiyama, A., 2009. Numerical calculations on countercurrent gas-liquid flow in a PWR hot leg (2) steam-water flow under PWR plant conditions. In: *Proceeding of the 13th International Topical Meeting on Nuclear Reactor Thermal Hydraulics (NURETH-13)*, Kanazawa City, Japan, September 2009.
- Lee, S.C., Bankoff, S.G., 1983. Stability of steam-water counter-current flow in an inclined channel: flooding. *Journal of Heat Transfer* 105, 713–718.
- Lopez de Bertodano, M., 1994. Counter-current gas-liquid flow in a pressurized water reactor hot leg. *Nuclear Science and Engineering* 117, 126–133.
- Menter, F., 1993. Zonal two-equation $k-\omega$ turbulence models for aerodynamic flows. *AIAA Journal* 93, 2906.
- Menter, F., 2002. CFD best practice guidelines for CFD code validation for reactor safety applications. ECORA FIKS-CT-2001-00154.
- Minami, N., Utanohara, Y., Kinoshita, I., Murase, M., Tomiyama, A., 2009. Numerical calculations on countercurrent gas-liquid flow in a PWR hot leg (1) air-water flow in a 1/15-scale model. In: *Proceeding of the 13th International Topical Meeting on Nuclear Reactor Thermal Hydraulics (NURETH-13)*, Kanazawa City, Japan, September 2009.
- Minami, N., Nishiwaki, Nariyai, T.D., Tomiyama, A., Murase, M., 2010a. Countercurrent gas-liquid flow in a PWR hot leg under reflux cooling (I) air-water tests for 1/15-scale model of a PWR hot leg. *Journal of Nuclear Science and Technology* 47 (2), 142–148.
- Minami, N., Murase, M., Tomiyama, A., 2010b. Countercurrent gas-liquid flow in a PWR hot leg under reflux cooling (II) numerical simulation of 1/15-scale air-water tests. *Journal of Nuclear Science and Technology* 47 (2), 149–155.
- Montoya, G.A., Deendarlianto, Lucas, D., Höhne, T., Vallée, C., 2011. Time dependent interfacial behavior during counter-current gas-liquid two-phase flow in a model of the hot leg of pressurized water reactor (PWR). In: *19th International Conference on Nuclear Engineering (ICONE)*, Chiba, Japan, 16–19 May 2011.
- Murase, M., Utanohara, Y., Kinoshita, I., Minami, N., Tomiyama, A., 2009. Numerical calculations on countercurrent air-water flow in small-scale models of a PWR hot leg using a VOF model. In: *Proceeding of the 17th International Conference on Nuclear Engineering (ICONE 17)*, Brussels, Belgium, July 2009.
- Nariyai, T., Tomiyama, A., Vallée, C., Lucas, D., Murase, M., 2010. Countercurrent flow limitation in a scale-down model of a PWR hot leg. In: *Proceeding of the 8th International Topical meeting on Nuclear Thermal-Hydraulics, Operation and Safety (NUTHOS-8)*, Shanghai, China, October 2010.
- Ohnuki, A., 1986. Experimental study of counter-current two-phase flow in horizontal tube connected to inclined riser. *Journal of Nuclear Science and Technology* 23 (3), 219–232.
- Ohnuki, A., Adachi, H., Murao, Y., 1988. Scale effects on countercurrent gas-liquid flow in a horizontal tube connected to an inclined riser. *Nuclear Engineering and Design* 107, 283–294.
- Prasser, H.M., Beyer, M., Carl, H., Manera, A., Pietruske, H., Schutz, H., Weiss, F.P., 2006. The multipurpose thermal hydraulic test facility TOPFLOW: an overview on experimental capabilities, instrumentation and result. *Kerntechnik* 71, 163–173.
- Utanohara, Y., Kinoshita, I., Murase, M., Minami, N., Tomiyama, A., 2009. Effects of interfacial friction correlations on numerical calculations for countercurrent gas-liquid flow in a PWR hot leg. In: *Proceeding of the 13th International Topical Meeting on Nuclear Reactor Thermal Hydraulics (NURETH-13)*, Kanazawa City, Japan, September 2009.
- Vallée, C., Deendarlianto, Beyer, M., Lucas, D., Carl, H., 2009a. Air/water counter-current flow experiments in a model of the hot leg of a pressurized water reactor. *Journal of Engineering for Gas Turbines and Power – Transactions of the ASME* 131, 022905.
- Vallée, C., Seidel, T., Lucas, D., Beyer, M., Prasser, H.-M., Pietruske, H., Schütz, P., Carl, H., 2009b. Influence of the fluid properties on co-current two-phase flows in a horizontal channel connected to a riser. In: *Proceedings of the 7th World Conference on Experimental Heat Transfer, Fluid Mechanics and Thermodynamics (ExHFT-7)*, Krakow, Poland, 28 June–03 July 2009, pp. 443–452.
- Vallée, C., Seidel, T., Lucas, D., Tomiyama, A., Murase, M., 2011. Comparison of counter-current flow limitation experiments performed in two different models of the hot leg of a pressurized water reactor with rectangular cross-section. *Journal of Engineering for Gas Turbines and Power – Transactions of the ASME* 133 (5) (article 052917).
- Wallis, G.B., 1969. *One-dimensional Two-phase Flow*. McGraw Hill, New York.
- Wang, M.J., Mayinger, F., 1995. Simulation and analysis of thermal-hydraulic phenomena in a PWR hot leg related to SBLOCA. *Nuclear Engineering and Design* 155, 643–652.
- Wongwises, S., 1996. Two-phase countercurrent flow in a model of a pressurized water reactor hot leg. *Nuclear Engineering and Design* 166 (2), 121–133.
- Yadigaroglu, G., 2005. Computational fluid dynamics for nuclear applications: from CFD to multi-scale CFMD. *Nuclear Engineering and Design* 235, 153–164.
- Yegorov, Y., 2004. Contact condensation in stratified steam-water flow. *EVOL-ECORA-D07*.